Surface and grain boundary segregation in 16MND5 steel

Tangui Morvan, Patrick Ganster, Vincent Barnier, Krzysztof Wolski

Surface and grain boundary segregation in 16MND5 steel

Tanguy Morvan, Patrick Ganster,* Vincent Barnier and Krzysztof Wolski

An adequate model of quantification when there are many segregating elements is required for industry and research. Hence, for the first time, surface segregation kinetics on industrial 16MND5 steel was studied by XPS spectroscopy at temperatures ranging from 500 to 600 °C. From measurements that highlight the competitive segregation of P, S, Sn, Sb, As, and Cu impurities at the surface, a quantification model was developed and successfully used to deduce the surface concentrations during segregation kinetics as well as derive the corresponding diffusion coefficients. We observed that phosphorus and sulfur are the first elements covering the surface, then they are supplanted by others' impurities. This result may reflect impurities segregation behavior at the grain boundaries that impacts mechanical behavior of the material. Indeed, to further the research, 16MND5 samples were aged in the same range of temperatures. Then, Auger spectroscopy measurements at grain boundaries were conducted on broken samples exhibiting intergranular cracking. Results show that phosphorus is the only segregating element present at grain boundaries after 2 months of aging. Importantly, it appears that phosphorus grain boundary segregation kinetics is significantly lower than at surface.

Keywords: segregation; steel; impurities

Introduction

For decades, impurities in steels (Sb, As, Sn, P, and S, …) are well known to segregate at surface and interfaces during tempering and/or during lifetime of the material and to affect its mechanical properties.

Phosphorus and sulfur are particularly worrying as these elements have been identified to corrupt the material and result in grain boundary embrittlement.[1–8]

This segregation alters the mechanical properties of materials. Many impurities segregation studies have been made on binary or ternary systems (i.e. solvent-solute) to identify the most detrimental ones.[9–12] Current methods are to use *ab initio* calculations to catch effect of impurities on the grain boundaries cohesion.[13–17] However, such techniques limit the number of grain boundary configurations that can be explored in reasonable amount of time. A better approach is required for industrial applications.

In comparison with relatively easy to study high-purity model alloys containing selected and controlled impurities, dealing with equilibrium surface and/or grain boundary segregation in industrial steels is far more challenging task. First, this is owing to the large number of possible segregating elements that diffuse at different time-scales. Second, there are multiple possible site competition at interfaces that can be combined with the solute interactions.[18–22]

16MND5 steel (A508 class 3) used in French nuclear reactors pressurized vessels was chosen to be studied because it is an excellent candidate containing a lot of impurities subject to segregation. In addition, it is crucial in nuclear reactors to understand how any possible embrittlement can occur. Accurate lifetime predictions and modeling of these vessels require an adequate knowledge of the intrinsic phenomena. To understand the cause of brittle fractures, studying inter-granular segregation kinetics and quantifying segregating elements are key issues to evaluate the role of impurities in embrittlement. Regarding 16MND5 steels possible embrittlement by phosphorus, Pineau *et al.* clearly highlight a grain boundary coverage threshold (0.1 monolayers) for the occurrence of inter-granular fracture associated with a decrease of the critical fracture stress.[23,24]

Our purpose is to use XPS and Auger electron spectroscopies (AES) to identify segregating elements and their segregation kinetics at surface and at grain boundaries in 16MND5 steel.

Surface segregation is observed by XPS spectroscopy with *in situ* heating of samples at 500, 550, and 600 °C. From a quantization model detailed later, the surface coverage of each elements during the segregation kinetics are evaluated. The diffusion coefficients of segregating elements are therefore deduced in 16MND5 steel. Grain boundary segregation is analyzed via the use of aged samples at 500 °C from 1 week to 3 months. Then, the latter are broken at low temperature to reveal grain boundaries and to analyze segregated elements by AES.

The rest of the article is organized as follows:

After a brief presentation of the material and methods, the first section presents surface segregation kinetics obtained by XPS measurements and the associated quantification model to deduce evolution of impurity distribution. The second reports grain boundary segregation using AES on aged samples. Finally, conclusions and remarks are suggested.

*Correspondence to: Patrick Ganster, Mines Saint-Etienne, Centre SMS, Laboratoire Georges Friedel, CNRS UMR5307, 158 Cours Fauriel, 42023 Saint-Etienne, France. E-mail: ganster@emse.fr

Mines Saint-Etienne Centre SMS, Laboratoire Georges Friedel, CNRS UMR5307, 158 cours Fauriel, 42023 Saint-Etienne, France

Material and experiments

Material

16MND5 steel (A508-class 3) is a low-alloyed bainitic steel mainly used as structural material in nuclear power plants. The material used in this study comes from scrap obtained after forging and heat processing reactor material. The composition was determined by Glow Discharge Mass Spectrometry (Table 1). Note that owing to chemical heterogeneities of the initial ingot (macrosegregation), the composition in the present material may sightly differ from those encountered in other studies.[24,27,28]

Figure 1 shows the microstructure of the material after mirror polishing and etching with Dino (left) and Nital (right) solutions.[25,26] The Dino etching illustrates that the primary austenitic grains are 20–25 μm diameter size (surrounded with thick lines in the figure). Treatment with Nital demonstrates that bainitic-like structure of the 16MND5 steel is characterized by oriented sub-structures in the primary austenitic grains. In the present 16MND5 material, Nital does not reveal any microsegregation.

XPS measurements

The X-ray photo-electron spectroscopy (XPS) measurements were carried out with a *Thetaprobe ThermoVG* system using an Al K non-monochromatized X-ray source and a hemispherical analyzer with a pass energy of 1 eV. The stage in the analysis chamber in ultra high vacuum ($< 10^{-9}$ mbar) has an *in situ* heating device, allowing to reach a maximum temperature of 650 °C.

Surface segregation kinetics at 500, 550, and 600 °C were measured with the following protocol. For each of these three temperatures, a fresh mirror-polished (1/4 μm grade) sample of 8-mm diameter and 500-μm thick is used. In the analysis chamber, after a initial degassing stage at 300 °C (2 h), the sample is quickly heated to the desire temperature in less than 10 min. Before recording any data, Argon ion sputtering was carried out for 3 min using 3 keV Ar^+ onto 1 mm^2 restricted area with 100 $\mu A \cdot cm^{-2}$ current density and 45° incident angle. These conditions were sufficient to remove the native oxide layer naturally present on the steel surface. Then, XPS spectra are recorded once each hour for 120 h to evaluate the kinetics of each segregating element.

Table 1. composition Chemical composition of 16MND5 steel sample obtained by Glow Discharge Mass Spectrometry (GDMS)

	Fe	C	Mn	Ni	Mo	P	Cr
wt%	bal.	0.14	1.40	0.66	0.54	0.0070	0.17
at. %	bal.	0.64	1.41	0.63	0.31	0.0126	0.18
	Cu	As	Sn	Sb	S		
wt%	0.079	0.0072	0.0045	0.0008	< 0.0008		
at.%	0.069	0.0053	0.0021	0.0003	< 0.0013		

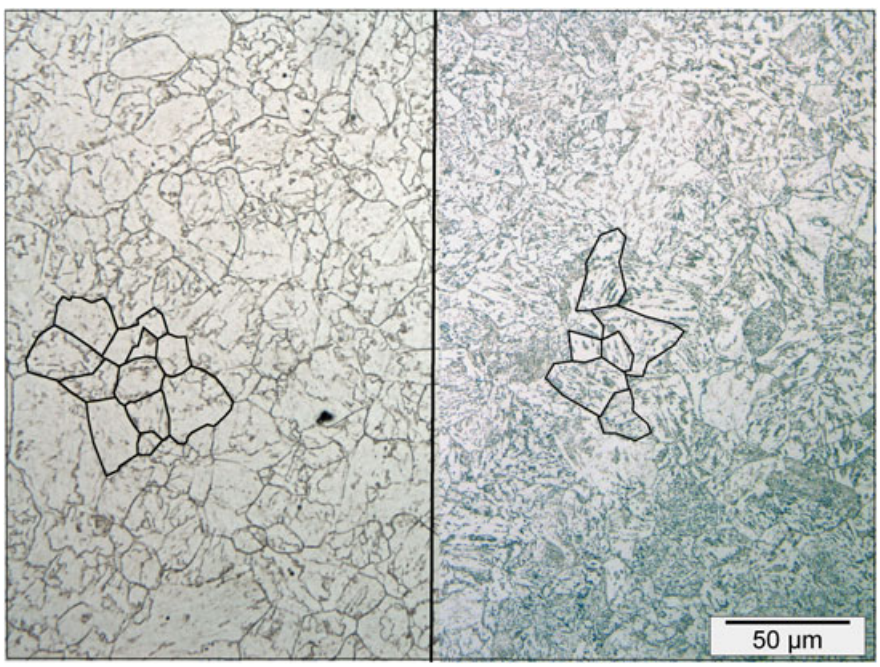

Figure 1. Optical observation of 16MND5 steel microstructure revealed by DINO (left) and Nital (right) solutions. Primary austenitic grain boundaries are marked by black thick lines. [Colour figure can be viewed at wileyonlinelibrary.com]

Figure 2 presents the XPS spectra obtained after a segregation kinetics at 600 °C (top spectrum) as compared with before (bottom spectrum).

After 120 h at 600 °C, the XPS spectrum shows that the main segregated elements on the surface are S, As, Sn, Sb, and Cu. At this stage, Phosphorus is not present anymore as its signal appears and finally disappears at the beginning of the segregation kinetics (next part).

Data are sequentially recorded in the energy window of each element. Each time, peak intensity of individual elements is determined using Shirley inelastic background subtraction.[29] Figure 3 presents the corresponding evolution of peak intensity for P, S, Sn, Sb, As, and Cu during segregation experiments at 500, 550, and 600 °C. Owing to the large number of elements that segregate, evolution of the peak intensities shows non-monotonous behaviors indicating competitive segregation during kinetics. At 600 °C, the effect is well established as the kinetics is sufficiently fast to almost reach equilibrium at the end of the experiment. Copper and phosphorus are the first elements to appear at the surface. Phosphorus is then fully supplanted by the other elements (S, As, Sn, Sb, and Cu) after few hours. The effect is characterized by the appearance and then disappearance of P signal during this period.

The same tendency appears at lower temperature (550 and 500 °C) despite that equilibrium is never reached owing to the slow kinetics. It is interesting that copper, which is usually considered as an alloying element, in this case is subject to segregation. At 600 °C, a decrease of the Cu signal at short time before it stabilization is observed. At 550 °C, the increase and decrease of the Cu peak before its stabilization indicate a tendency to segregate at the surface. Note: the Cu is never fully supplanted by the other segregating elements. Moreover, Cu peak intensity stabilizes in the same range of values at 550 and 600 °C. This indicates that Cu would remain in the segregation layer or subsurface. At 500 °C, surface equilibrium is not reached nor the Cu stabilized.

In order to quantify the elements in the segregation layer, a model to deduce surface concentrations is proposed in the next section.

Quantification model

From the peak intensities, we require a model to quantify surface concentration during segregation kinetics and deduce diffusion

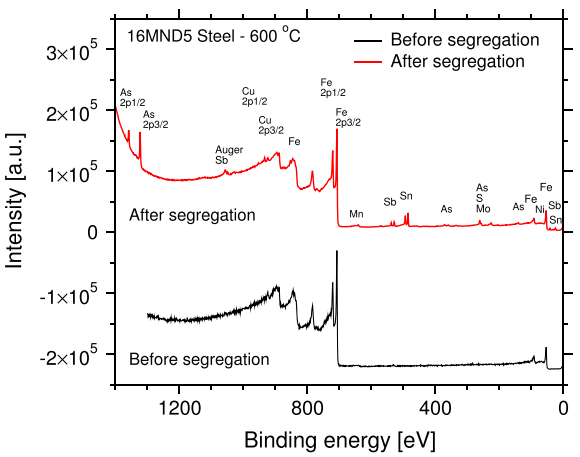

Figure 2. Full XPSspectra acquired on mirror polished 16MND5 steels after 120 h at 600 °C (top spectra) and before (bottom). [Color figure can be viewed at wileyonlinelibrary.com]

properties of the elements involved. Our first assumption considers that the segregating elements would form a segregation mono-layer at the 16MND5 steel surface. We simplify this steel to a pure iron matrix. This surface monolayer contains a mixture of segregating elements, and their coverage on the iron matrix is denoted by τ (a value between 0 and 1 representing the fraction of segregation sites occupied by all segregated species). Their coverage obscures the iron peak signal.

A schematic cross section of the segregation monolayer on the top of iron matrix is presented in Figure 4. Part of the iron signal is attenuated by the segregated elements (coverage τ), whereas the other one is not.

Peak intensity of the segregating atoms (x =P, S, As, Sn, Sb, or Cu) in the top mono-layer can be expressed as

$$I_x^{XPS} = SFT_x\sigma_x c_x \tag{1}$$

where S is the surface analyzed, F the photon flux, T_x the analyzer transmission function, σ_x the photo-ionization cross section of element x, and c_x atomic surface concentration in at.cm^{-2}.

Taking into account, the presence of the segregated elements on the surface with τ, the iron XPS peak intensity derived from a mono-layers decomposition of the substrate (numbered by the index i in Fig. 4 is

$$I_{Fe}^{XPS} = SFT\sigma_{Fe}N_{Fe}\left[1-k_{Fe}^{Fe}\right]\lambda_{Fe}^{Fe}\cos\theta \tag{2}$$

$$\times\left((1-\tau)+\tau k_{Fe}^{0}\right)\sum_{i=1}^{\infty}(k_{Fe}^{Fe})^{i-1} \tag{3}$$

where F is the photon flux, T the analyzer transmission function, N_{Fe} the atomic concentration of iron that is assumed to be constant in the mono-layers. Then, $k_{Fe}^{Fe} = \exp(-\frac{d}{\lambda_{Fe}^{Fe}\cos(\theta)})$ is the attenuation factor of iron photoelectrons through an iron mono-layer of d thickness (d correspond to a mono-layer thickness assumed as $d \sim (a_0^3/2)^{1/3}$ where a_0 is the $\alpha-$iron lattice parameter, i.e. d = 2.28 Å), λ_{Fe}^{Fe} = 13 Å is the inelastic mean free path for iron photoelectrons in the iron matrix and $k_{Fe}^{0} = \langle k_{Fe}^{i}\rangle_{i=\text{P, Sn, Sb, As, S, Cu}} \sim 0.83$ is a mean attenuation factor of iron photoelectrons through the segregated monolayer where k_{Fe}^{i} corresponds to the attenuation factor of iron photoelectrons in a mono-layer of the i element. Values for the mean free path λ_{Fe}^{i} to define the attenuation factor $k_{Fe}^{i} = exp(-\frac{d}{\lambda_{Fe}^{i}\cos\theta})$ for the segregating elements P, S, Sn, Sb, As, and Cu are 20, 20, 19, 19, 18, and 13 Å, respectively.[30] Analysis angle of our XPS analyzer is $\theta = 50^o$. From Scofield tabulation[31], Photo-ionization cross sections σ are 10.82, 27.19, 25.05, 27.74, 1.19, and 16.73 in terms of C*1s* cross section for Fe, As, Sn, Sb and P, and Cu, respectively. Iron mono-layers are sufficiently thin to allow a Taylor expansion of k_{Fe}^{Fe} (i.e. $k_{Fe}^{Fe} = \exp(-\frac{d}{\lambda_{Fe}^{Fe}\cos(\theta)}) \sim 1-\frac{d}{\lambda_{Fe}^{Fe}\cos(\theta)}$) that simplifies the aforementioned expression as

$$I_{Fe}^{XPS} = FT_{Fe}c_{Fe}\sigma_{Fe}[(1-\tau)+\tau k_{Fe}^{0}]\sum_{i=1}^{\infty}(k_{Fe}^{Fe})^{i} \tag{4}$$

$$= FT_{Fe}c_{Fe}\sigma_{Fe}\frac{(1-\tau)+\tau k_{Fe}^{0}}{1-k_{Fe}^{Fe}} \tag{5}$$

where $c_{Fe} = N_{Fe}d$ corresponds to the iron surface concentration. (Assuming the mass density of 16MND5 steel is close to 7.8 g·cm^{-3} and a mean monolayer thickness of 2.28 Å, $c_{Fe} = 1.92 \times 10^{15}$ at.cm^{-3})

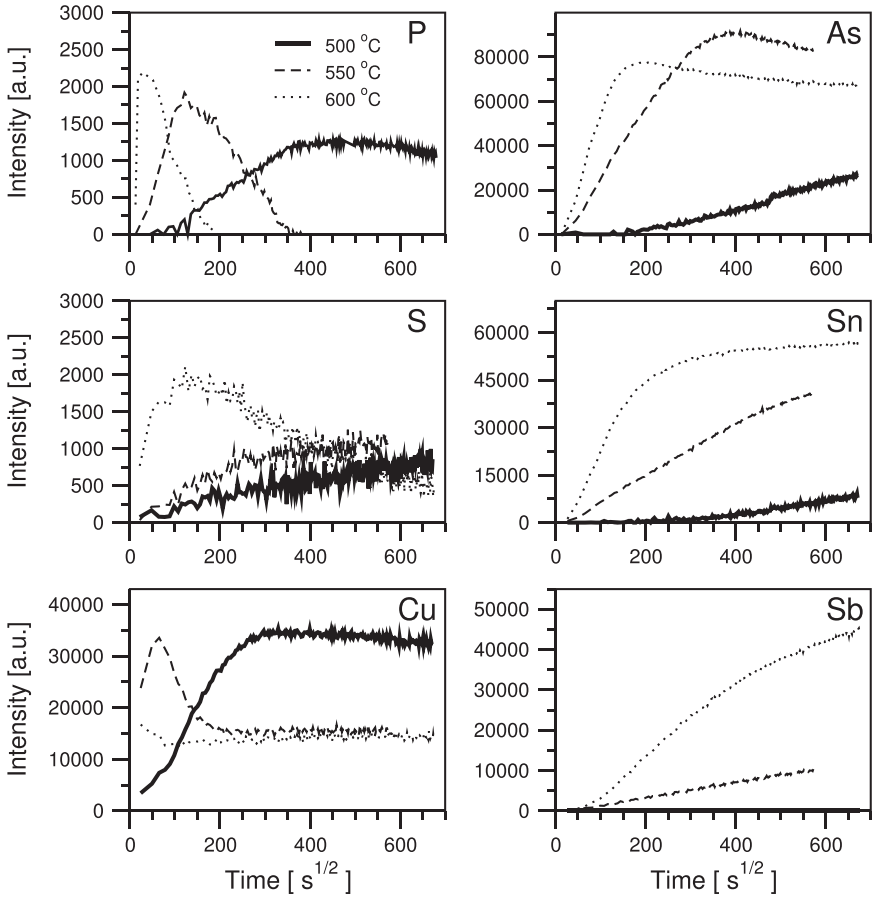

Figure 3. (colored online) Kinetics of surface segregation for P, S, Cu, As, Sn, and Sb at 500, 550, and 600 °C in 16MND5 steel. The results highlights the competitive behavior of all these elements where Cu and P are the first elements to reach the surface.

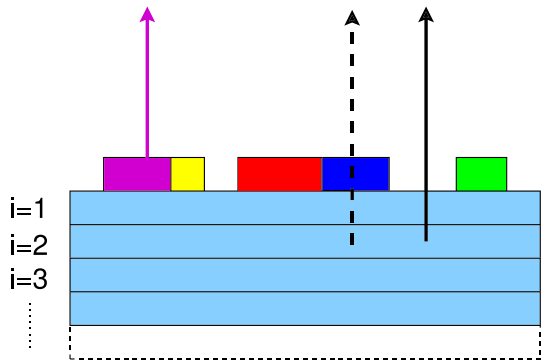

Figure 4. Cross section showing segregating atoms that form a top mono-layer on the sample. Segregating elements and iron XPS peak intensities are derived from the discrete summation of the mono-layers contribution in the substrate. The short solid arrow illustrates signal of the mixed segregated elements on the surface. The long solid arrow denotes the iron signal from the uncovered part. The long dashed arrow demonstrates the covered one. [Color figure can be viewed at wileyonlinelibrary.com]

Assuming that the coverage expressed as $\tau = \frac{c_P+c_S+c_{As}+c_{Sb}+c_{Sn}}{c_{Fe}e}$, the peak ratio of the segregated elements over iron ($\theta_x^{XPS} = \frac{I_X}{I_{Fe}}$) leads to a set of equations that can be used to deduce the surface concentration of each segregated element. By defining $\alpha_x = \frac{T_x\sigma_x(1-k_{Fe}^{Fe})}{T_{Fe}\sigma_{Fe}(1-k_{Fe}^{0})}$ where x = P, S, As, Sb, Sn, and Cu, the set of equations in matrix form can be written thus:

$$M.c_i = \frac{1}{1-k_{Fe}^{0}}c_{Fe} \tag{6}$$

where

$$M = \begin{pmatrix} \frac{\alpha_P}{\Theta_P}+1 & 1 & 1 & 1 & 1 & 1 \\ 1 & \frac{\alpha_S}{\Theta_S}+1 & 1 & 1 & 1 & 1 \\ 1 & 1 & \frac{\alpha_{As}}{\Theta_{As}}+1 & 1 & 1 & 1 \\ 1 & 1 & 1 & \frac{\alpha_{Sb}}{\Theta_{Sb}}+1 & 1 & 1 \\ 1 & 1 & 1 & 1 & \frac{\alpha_{Sn}}{\Theta_{Sn}}+1 & 1 \\ 1 & 1 & 1 & 1 & 1 & \frac{\alpha_{Cu}}{\Theta_{Cu}}+1 \end{pmatrix}$$

and c_i is a column vector of the segregating element concentrations and c_{Fe} is a column vector of the iron concentration that is assumed to be constant.

Model application

From the XPS measurements of the segregation kinetics previously presented in Fig. a, surface concentration of segregated elements are deduced by reversing equation 6 using scilab software.[32]

All segregation kinetic curves of Fig. a were therefore fitted by polynomial functions and then discretized to obtain intensities at same times. Figure 5 presents the evolution of surface concentrations of the segregating elements as a function of $t^{1/2}$ derived from the quantification model.

Results show that the segregation monolayer is mainly composed of P briefly with a maximum coverage of around 0.25 at 600 °C. Phosphorus is the first impurity to reach and to cover the surface before being supplanted by the other elements. The segregation monolayer is finally composed of several impurities.

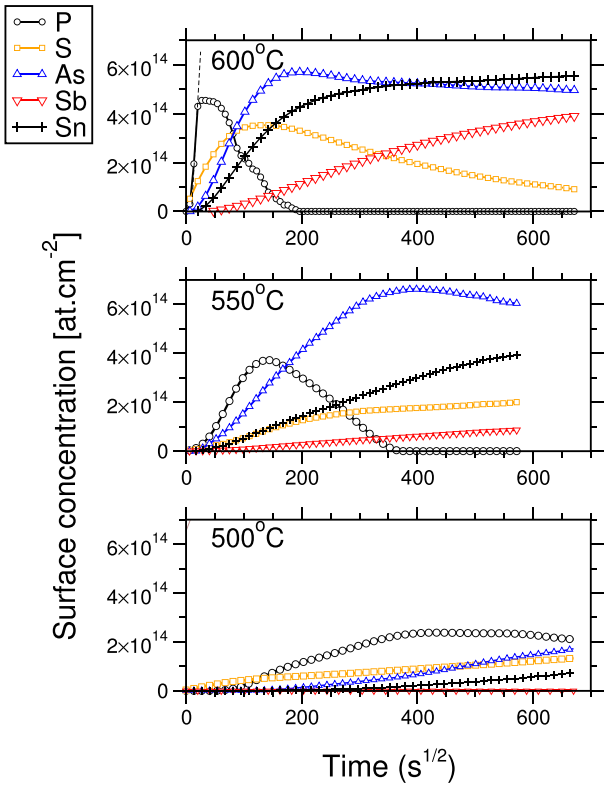

Figure 5. The evolution of P, S, Sn, Sb, and As surface concentrations as a function of time at 600, 550, and 500 °C deduced from our quantitative model. [Color figure can be viewed at wileyonlinelibrary.com]

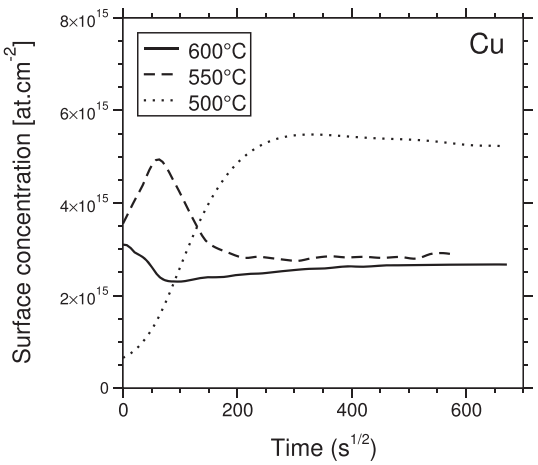

Figure 6. Evolution of Cu surface concentration as a function of the time at 600, 550, and 500 °C deduced from the proposed quantitative model.

Regarding Cu surface concentrations over time in Figure 6, it appears that Copper surface concentrations are significantly higher than the other impurities and even more than irons ($\sim 1.9\times10^{15}$ at.cm $^{-2}$). While this may indicate the limits of our model assumption of only one segregation layer; however, the values given for the five segregated species have staid valid. Regarding copper, it certainly extends outside of this segregation layer to the interior.

Kinetics of segregation

According to the McLean's model[33] (impurities in a solid solution), the initial stage of impurity segregation kinetics can be described by the following relationship:

$$x_l^{surf}(t) = \frac{2x_l^{bulk}}{\delta}\sqrt{\frac{D_l t}{\pi}} \tag{7}$$

where x_l^{surf} is the concentration in $at.cm^{-3}$ of the segregating element in the segregation monolayer with the thickness δ , x_l^{bulk} the impurity concentration in bulk, and D_l the impurity effective diffusion coefficient.

This expression can thus be expressed in surface concentration unit (at.cm^{-2}) by multiplying it by δ.

$$c_l^{surf}(t) = 2\times_l^{bulk}\sqrt{\frac{D_l t}{\pi}} \tag{8}$$

where c_l is the surface concentration of the *l* impurity.

Owing to the difficulty to deduce the linear part at the initial stage of the kinetics, we present in Fig. 7 evolution of the diffusion coefficients ($D_l^* = \pi(\frac{c_l^{surf}(t)}{2\times_l^{bulk}})^2$ derived in reversing Eq.8). It shows that they cover a large range of values with high incertities. The mean values and root-mean-squared deviations are resumed in Table 2.

The small temperature range investigated does not allow us to extract reliable diffusion coefficient prefactors nor activation energies. This is not the case in literature. Diffusion properties are derived from model steels and high purity iron[34–38] for higher temperatures. However, our problem deals with complex industrial conditions. Note: the range of diffusion coefficient values are only in accordance at 550 °C. Indeed, our results tend to underestimate diffusion coefficients at 500 °C and overestimate them at 600 °C. Any discrepancy with literature can be attributed to the complex microstructure of 16MND5 steel where it exists uncertainties on x_l^{bulk} owing to heterogeneities at differing scales. Moreover, the scope of this study does not take into account the interactions between the elements.

To compare the surface and grain boundary segregation kinetics, the next section investigates Auger spectroscopy measurements at grain boundaries.

Segregation kinetics at grain boundaries

In surface segregation, phosphorus appears to be the first 16MND5 impurity to partially cover the surface, reaching a maximum value before being supplanted by others' impurities. The study of Naudin *and al.* [24] clearly highlights the effect of phosphorus content at grain boundary on mechanical properties of 16MND5 steels after diverse heat treatments and cooling

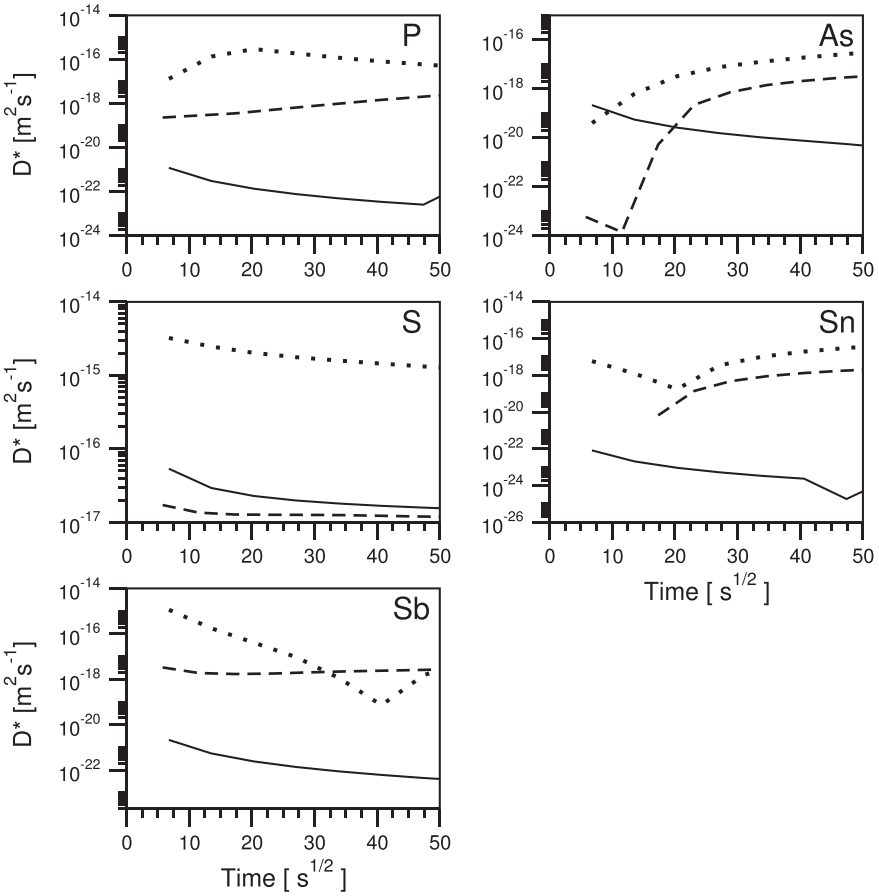

Figure 7. Evolution of the diffusion coefficients for P, S, As, Sn, Sb at 500, 550, and 600 °C deduded from MacLean's equation at the starting of the kinetics.

Table 2. Average and root-mean-squared deviations diffusion coefficients of segregating 16MND5 impurities at 500, 550, and 600 °C derived from surface segregation kinetics measured by XPS (in $m^2 \cdot s^{-1}$).

	500 °C	550 °C	600 °C
P	$2.6 \times 10^{-22} \pm 4.3 \times 10^{-22}$	$9.2 \times 10^{-20} \pm 4.3 \times 10^{-19}$	$1.3 \times 10^{-16} \pm 9.3 \times 10^{-17}$
S	$1.3 \times 10^{-17} \pm 1.7 \times 10^{-18}$	$2.5 \times 10^{-17} \pm 1.3 \times 10^{-17}$	$9.8 \times 10^{-16} \pm 6.7 \times 10^{-16}$
As	$4.8 \times 10^{-20} \pm 7.6 \times 10^{-20}$	$9.1 \times 10^{-19} \pm 1.8 \times 10^{-18}$	$1.0 \times 10^{-17} \pm 1.0 \times 10^{-17}$
Sb	$4.7 \times 10^{-22} \pm 7.6 \times 10^{-22}$	$2.2 \times 10^{-18} \pm 5.4 \times 10^{-19}$	$2.0 \times 10^{-18} \pm 5.4 \times 10^{-19}$
Sn	$1.8 \times 10^{-23} \pm 2.9 \times 10^{-23}$	$7.7 \times 10^{-19} \pm 6.9 \times 10^{-19}$	$1.0 \times 10^{-17} \pm 1.1 \times 10^{-17}$

procedures. In their study, phosphorus is the only impurity included in 16MND5 grain boundaries. Therefore, to evaluate the grain boundary segregation kinetics, 1 mm×1 mm×24 mm sized 16MND5 samples were aged in Ar atmosphere (in sealed quartz tubes) for 1–3 weeks and 1–3 months at 500 °C. Each sample aged was then cooled to −120 °C, then fractured in ultra high vacuum within the preparation chamber of our Auger analyzer. Under such experimental conditions, brittle fractures are obtained. The fracture surface of samples are then observed using secondary electrons to identify the presence of intergranular cracking. Then, AES was performed with the same instrument using a field emission electron gun operating at 10 kV accelerating voltage with a 5 nA beam current and a 45° tilt, resulting in a 150 nm effective spot.

Figure 8 presents the surfaces of 16MND5 steels after the impact at low temperature for the cases of intragranular and intergranular fractures. The samples were broken well below the brittle-ductile transition temperature[39] to ensure a brittle fracture.

For intragranular fracture, the fracture surface is characterized by a step-like structure of the surface owing to cleavage (Fig. 8 top). 16MND5 intergranular cracking areas are characterized by the presence of grain edges associated with a rough surface (surrounded by thick lines in Fig. 8 bottom). The typical size of the intergranular facet is 10Ů20-μm diameter corresponding to the austenitic grain size.

When Intergranular cracking appeared, after 2 months of aging at 500 °C, then Auger electron spectroscopy was conducted on

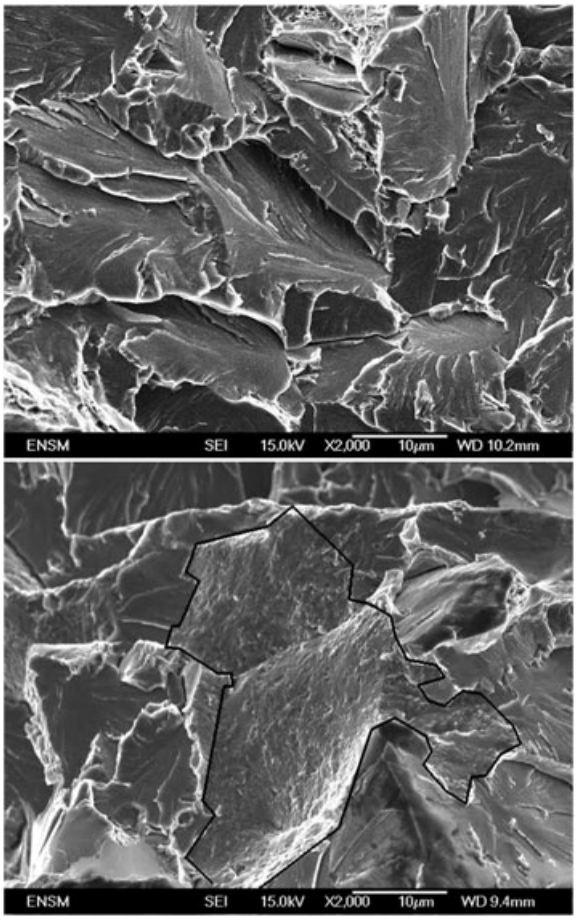

Figure 8. Fracture surface in the case of 16MND5 cleavage (top) and in the case of intergranular fracture (bottom). Some intergranular surfaces are surrounded by a black line.

those intergranular areas revealed. Figure 9 shows AES spectra acquired on intergranular cracking areas. The spectra show that presence of Fe, P, C, and O elements in grain boundaries. The 120 eV peaks corresponds to P element, the 48 and 703 eV peaks correspond to the Fe matrix. The peaks at 280 and 403 eV result from the contamination of the vaccuum chamber with C and O, respectively. Note that part of the C signal could be attributed to cementite and/or a segregating C element.

Phosphorus (τ) at grain boundaries calculated with the model developed in Quantification Model Section is 0.03 and 0.08 for 2 and 3 months of aging at 500 °C, respectively. To compare with litterature, the phosphorus grain boundary concentrations are also derived from the model developed by Seah and Briggs[40,41] given by the following expression, $C_P = 1.13\ I_P/I_{Fe703}$ where I_P and I_{Fe703} correspond to the peak-to-peak heights of P peak at 120 eV and Fe peak at 703 eV deduced from derived spectra. At the aging temperature of 500 °C, phosphorus at grain boundaries is 0.04 and 0.12 vol.% for 2 and 3 months of aging time, respectively. This result is in accordance with Naudin *et al.* because the small concentration of phosphorus, which increases with aging, is correlated with the few intergranular areas present on the grain boundary revealed. The number of intergranular areas increases as well when increasing heat treatment duration up to 3 months. At this aging stage, only the phosphorus impurity is present at grain boundary. Assuming that the order of appearance of

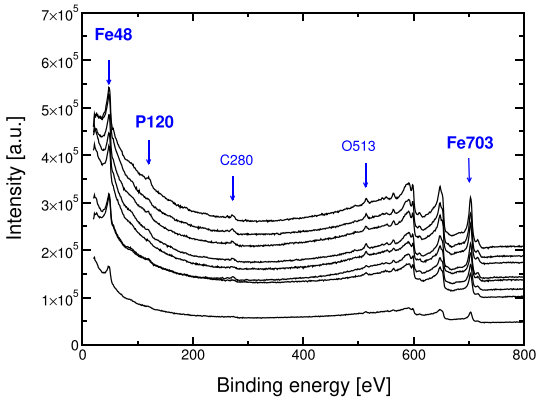

Figure 9. Auger spectra recorded on intergranular facets of 16MND5 steel aged at 500 °C for 3 months. [Colour figure can be viewed at wileyonlinelibrary.com]

segregating elements is the same as at the surface, the grain boundary segregation kinetics appears to be significantly slower than at surfaces because only phosphorus is present. This assumption means that in sufficiently advanced segregation kinetics, sulfur would be at least expected. This effect might be explained by the fact that a large part of diffusion processes for the surface segregation is driven by grain boundaries that act as diffusion short-circuits, whereas the diffusion processes for grain boundary segregation correspond to bulk diffusion.

Conclusion

The impurity segregation kinetics of 16MND5 steel was studied by means of XPS (surface) and AES (grain boundary). Surface segregation kinetics obtained by XPS measurements have shown that phosphorus is the first impurity element that reaches the surface before being supplanted by the others impurities S, As, Sn, and Sb. Copper that is an alloying element is also segregating at the surface. From XPS quantification model, surface concentration evolution was used to deduce impurity diffusion properties.

After aging at 500 °C, followed by *in situ* fracture below the brittle-ductile temperature transition, the 16MND5 steel began to reveal intergranular cracking behavior after 2 months. AES measurements on intergranular areas proved that phosphorus is the only segregating element present at the 16MND5 steel grain boundaries. Because of cost considerations, long-term aging is prohibitive. However, we can infer that the other impurities would segregate at the GB in a similar order as determined by XPS, therefore phosphorus segregation kinetics at GB should be significantly lower than at the surface at 500 °C.

Acknowledgements

We thanks AREVA NP to provide us the industrial grade of 16MND5 steel and enlightening discussions with F. Roch, P. Joly and A. Andrieu. Christopher Yukna for proof reading.

References

[1] M. P. Seah, *Surf. Science* **1975**, *53*, 168.
[2] J. R. Rice, J.-S. Wang, *Mat. Sci. Eng* **1989**, *A107*, 23.
[3] R. P. Messmer, C. L. Briant, *Acta Metall* **1982**, *30*, 467.
[4] M. Militzer, S. Hofmann, *Scripta Met. et Mat* **1994**, *31*, 1501.

[5] M. Yamagushi, Y. Nishiyama, H. Kaburaki, *Phys. Rev. B* **2007**, *76*, 035418.
[6] M. Paju, H. J. Grabke, *Materials Science and Technology* **1989**, *5*, 153.
[7] J. Ouder, Mater. Sci, *Eng* **1980**, *42*, 101.
[8] P. Lejcek, *Book: Grain Boundary Segregation in Metals*, Series in Mat. Science, Spring, Berlin, **2010**, pp. 136.
[9] M. C. Inman, H. R. Tripler, *Acta Metall* **1958**, *6*, 73.
[10] Rüsenberg and Viefhaus, *Surf. Sci* **1985**, *159*, 1.
[11] Dumoulin and Guttmann, *Mat. Sci. Eng* **1980**, *42*, 249.
[12] M. P. Seah, C. Lea, *Philos. Mag* **1975**, *31*, 627.
[13] F. Berthier, B. Legrand, G. Treglia, *Acta Mater* **1999**, *47*, 2705.
[14] M. Hashimoto, Y. Ishida, R. Yamamoto, M. Doyama, *Acta Metall* **1984**, *32*, 1.
[15] R. Wu, A. J. Freeman, G. B. Olson, *Science* **1994**, *265*, 376.
[16] L. Zhong, R. Wu, A. J. Freeman, G. B. Olson, *Phys. Rev. B* **2000**, *62*, 13938.
[17] L. Marbela, et al., *J. Nucl. Mat* **2010**, *406*, 7.
[18] C. Lea, M. P. Seah, *Surf. Sci* **1975**, *53*, 273.
[19] G. T. Burstein, J. Q. Clayton, Scripta Metal **1979**, *13*, 1099.
[20] A. V. Krajnikov, M. Militzer, J. Wieting, *Mat. Sci. and Tech* **1997**, *13*, 877.
[21] R. G. Ding, T. S. Rong, J. Knott, *Mat. Sc. and Tech* **2005**, *21*, 1255.
[22] H. Erhart, H. J. Grabke, *Metal Science* **1981**, *15*, 401.
[23] A. Tavassoli, P. Soulat, A. Pineau, *Book: Residual and Unspecified Elements in Steel,* ASTM STP 1042 (Ed: Melilli/Nisbett editors), **1989**.
[24] C. Naudin, J. M. Frund, A. Pineau, *Scripta Materiala* **1999**, *40*, 1013.
[25] Composition of Nital solution : 2 ml HNO_3, 98 ml ethanol.
[26] Composition of DINO solution : 140 ml distilled water, 100 ml H_2O_2 30%, 4 g oxalic acid, 2 ml H_2SO_4, 1.5 ml HF.
[27] L. Taleb, Materiaux 2002 Proceeding Conference, INSA de Rouen, **2002**.
[28] J. Mathieu, S. Berveiller, K. Inal, O. Diard, *17ieme Congres Francais de mecanique*, Troye, **2005**.
[29] D. A. Shirley, *Rev, Phys. B* **1972**, *5*, 4709.
[30] S. Tanuma, C. J. Powell, D. R. Penn, *Surf. Inter. Anal* **1994**, *21*, 165.
[31] J. H. Scofield, *Theoretical Photoionization Cross Sections from 1 to 1500 keV*, Lawrence Livermore National Laboratory Rep, UCRL-51326, **1973**.
[32] Scilab Enterprises, Scilab: Free and Open Source software for numerical computation (OS, Version 5.5) [Software], **2012**. Available from: http://www.scilab.org.
[33] D. McLean, *Grain Boundaries in Metals*, Oxford University Press, Oxford, **1957**.
[34] T. Matsuyama, H. Hosokawa, H. Suto, Trans, *Jap. Inst. Met* **1983**, *24*, 589.
[35] B. I. Bozic, R. J. Lucic, *J. Mat. Sc* **1976**, *11*, 887.
[36] G. A Bruggeman, J. A. Roberts, *Metal. Trans. A* **1975**, *6A*, 755.
[37] D. N. Torres, R. A. Perez, F. Dyment, *Acta. Mater* **2000**, *48*, 2925.
[38] R. A. Perez, D. N. Torres, F. Dyment, *Appl. Phys. A* **2005**, *81*, 787.
[39] P. Hausild, I. Nedbal, C. Berdin, C. Prioul, *Mat. Sci. Eng A* **2002**, *335*, 164.
[40] M. P. Seah, W. A. Dench, *Surf. and Int. Anal* **1979**, *1*, 2.
[41] D. Briggs, M. P. Seah, Practical surface analysis by Auger and X-ray photoelectron spectroscopy (Eds: D Briggs, M. P. Seah), John Wiley, **1983**.